*Chin. J. Chem. Eng.*, **15**(4) 499—506 (2007)

# An Improved Design of Spiral Groove Mechanical Seal

**ZHOU Jianfeng**(周剑锋)*, **GU Boqin**(顾伯勤) **and CHEN Ye**(陈晔)
Fluid Sealing and Control Laboratory, College of Mechanical and Power Engineering, Nanjing University of Technology, Nanjing 210009, China

**Abstract** The coupling effect among the flow of fluid film, the frictional heat of fluid film and the thermal deformation of sealing rings is inherent in mechanical seals. The frictional heat transfer analysis was carried out to optimize the geometrical parameters of the sealing rings, such as the length, the inner radius and the outer radius. The geometrical parameters of spiral grooves, such as the spiral angle, the end radius, the groove depth, the ratio of the groove width to the weir width and the number of the grooves, were optimized by regarding the maximum bearing force of fluid film as the optimization objective with the coupling effect considered. The depth of spiral groove was designed to gradually increase from the end radius of spiral groove to the outer radius of end face in order to decrease the weakening effect of thermal deformation on the hydrodynamic effect of spiral grooves. The end faces of sealing rings were machined to form a divergent gap at inner radius, and a parallel gap will form to reduce the leakage rate when the thermal deformation takes place. The improved spiral groove mechanical seal possesses good heat transfer performance and sealing ability.
**Keywords** spiral groove, mechanical seal, heat transfer, optimum design, bearing force, leakage rate

## 1 INTRODUCTION

The non-contacting and non-leaking mechanical seal with multiple lobe grooves on the end face of rotating ring was developed by Etsion in 1984[1] and Lai described the development of this kind of mechanical seals later[2]. The shallow grooves can generate hydrodynamic pressure of fluid film between the end faces of the rotating ring and the stationary ring[3]. The profile of the shallow groove may be spiral, radial, rectangular and so on. Among the log spiral and Archimedes' spiral, the log spiral is more effective than the later. The log spiral groove sealing ring is illustrated in Fig.1 and the log spiral is defined by Eq.(1):

$$r = R_g e^{\theta \tan \alpha} \tag{1}$$

The fluid film thickness and the groove depth are all of micron dimension.

The bearing force of fluid film in the spiral groove mechanical seal is much larger than that in flat end face mechanical seal. It changes with the fluid film thickness which is automatically adjusted to keep the balance between the bearing force of fluid film and the closing force provided by spring or bellow. The characteristics of fluid flow in ideal parallel gap have been paid more attention than the effect of deformation of the sealing rings on sealing performance[4—7]. But the experimental results showed that the load-carrying capacity depended significantly upon the deformation of the sealing members[8]. When the mechanical seal is running, the frictional heat of fluid film is generated continuously and the sealing performance is different from the design objective. Some investigators found that the frictional heat played a very important role in mechanical seals [9—13], and some discussed the thermo-hydrodynamic (THD) mechanism in mechanical seals[14—17]. The early researches noticed the effect of frictional heat on the sealing performance but none of them considered the coupling effect among the fluid flow, the heat transfer and the thermal deformation.

A coupling analysis of the fluid film and the sealing rings was put forward in this paper. An improved design of spiral groove mechanical seal based on THD was investigated to determine the geometrical parameters of the sealing members that correspond to the relative large bearing force of fluid film, the small

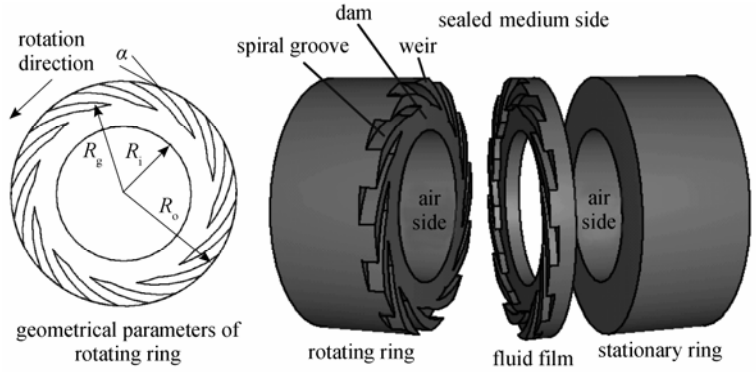


**Figure 1 Model of spiral groove mechanical seal**

Received 2006-09-06, accepted 2007-04-29.
* To whom correspondence should be addressed. E-mail: zhoujianfeng_ren@163.com

**Table 1 Material parameters of sealing rings**

| | Material | $E$, GPa | $\tau\times10^6$, $K^{-1}$ | $\lambda$, $W\cdot m^{-1}\cdot K^{-1}$ | $C$, $J\cdot kg^{-1}\cdot K^{-1}$ | $\varepsilon$ |
|---|---|---|---|---|---|---|
| rotating ring | stainless steel 316L | 200 | 16 | 16 | 502 | 0.30 |
| stationary ring | carbine graphite | 25 | 5 | 10 | 174 | 0.15 |

leakage rate and good heat transfer capability.

In this paper, the sealed medium is water, $\lambda=0.06W\cdot m^{-1}\cdot K^{-1}$, $\mu=0.001Pa\cdot s$, $\nu=1\times10^{-6}m^2\cdot s^{-1}$, $Pr=7.02$, $p_o=1MPa$. The materials of the sealing rings and their physical characteristics parameters are listed in Table 1.

## 2 HEAT TRANSFER IN SPIRAL GROOVE SEAL

### 2.1 Heat transfer model

The heat transfer system of spiral groove mechanical seal consists of the rotating ring, the stationary ring, the fluid film and the sealed medium. The axial cross section of the model of spiral groove mechanical seal in rectangular coordinate system is illustrated in Fig.2.

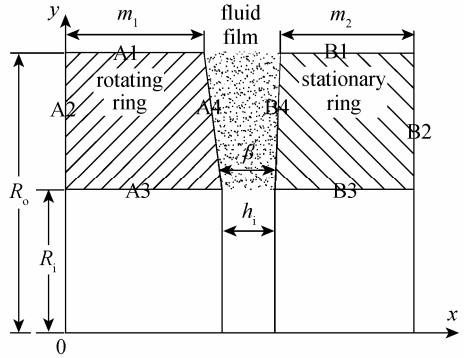


**Figure 2 Cross section of the model of spiral groove mechanical seal**

The symmetry axis $x$ is the rotating shaft and $y$ is the radial coordinate. Since the leakage rate of sealed medium through the gap composed by two end faces is very small, the frictional heat taken away by leakage can be neglected. The boundaries A2, A3, B2 and B3 connect with air, and the air is almost standing. Hence, the cooling effect of air is very weak and negligible, and the boundaries A2, A3, B2 and B3 were regarded as thermal isolation. The frictional heat of fluid film was assumed to conduct from boundaries A4 and B4 to A1 and B1, finally to sealed medium. Some other assumptions were made as follows:

(1) The temperature field and deformation were axisymmetrical in spite of the effect of spiral grooves.

(2) The sealed medium was Newtonian, and its viscosity remained constant in the direction of fluid film thickness but varied along radius.

(3) The temperature of the sealed medium $T_0$ was constant.

(4) The radial outlines of the two deformed end faces were approximately regarded as straight lines because the deformation is very small.

(5) The heat transfer took place under steady state.

The thickness of fluid film in non-groove and groove area can be expressed by Eqs.(2) and (3), respectively.

$$h_1(y)=h_i+(y-R_i)\tan\beta \tag{2}$$

$$h_2(y)=h_g+h_i+(y-R_i)\tan\beta \tag{3}$$

### 2.2 Frictional heat of fluid film

The frictional heat flux can be calculated by

$$q(y)=\mu_{(T_m)}\omega^2\frac{y^2}{h(y)} \tag{4}$$

where $\mu_{(T_m)}$ is the viscosity of fluid film determined by the mean temperature of fluid film $T_m$. For water, the relationship between its viscosity and temperature[15] can be expressed by

$$\mu_{(T_m)}=\mu_0\exp\left[-0.0175(T_m-T_0)\right] \tag{5}$$

where $\mu_0$ is the known viscosity corresponding to the temperature $T_0$.

### 2.3 Temperature field of sealing rings

The heat conductance model of a sealing ring is illustrated in Fig.3, and it is available for both rotating ring and stationary ring. $m$ is the length of the sealing ring and $n=R_o-R_i$. The heat transfer governing equation is in the form[18]

$$\frac{\partial^2T}{\partial x^2}+\frac{\partial^2T}{\partial y^2}=0 \tag{6}$$

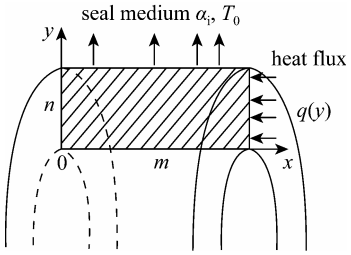


**Figure 3 Model of sealing ring**

Equation (7) can be obtained by using the boundary condition at $y=n$:

$$\frac{\lambda}{\alpha_i}k=\cot nk \tag{7}$$

Using the thermal insulation conditions at $x=0$ and $y=0$, the general solution of Eq.(6) was obtained to be

$$T(x,y)=\sum_{i=1}^{\infty}B_i\left(e^{k_ix}+e^{-k_ix}\right)\cos k_iy \tag{8}$$

where $k_i$ is the solution of Eq.(7) and $B_i$ is undetermined. According to the heat flux boundary condition at $x=m$, Eq.(9) was obtained.

$$\sum_{i=1}^{\infty} B_i k_i \left(\mathrm{e}^{k_i m} - \mathrm{e}^{-k_i m}\right)\cos k_i y = \frac{q}{\lambda} \tag{9}$$

where $q$ is the heat flux exerted on end face. For rotating ring, $q=\delta_1 q(y)$ and for stationary ring, $q=\delta_2 q(y)$. $\delta_1$ and $\delta_2$ are the heat distribution ratios for rotating ring and stationary ring respectively. The heat flux $q$ along axis $y$ is not continuous because of the influence of spiral grooves. But only when $q$ is a linear function of $y$, can Eq.(9) be solved. Therefore, some discrete values of $q_i$ and their corresponding $y_i$ were used to fit a liner function. Fig.4 illustrates a linear fitting example, $D_n$ is the serial number of the discrete values of $y_i$ from $y=0$ to $y=n$. When $y>R_\mathrm{o}-R_\mathrm{g}$,

$$q_i = \mu_{(T_\mathrm{m})}\omega^2 y^2\left[\frac{B}{h_2(y)} + \frac{1-B}{h_1(y)}\right]$$

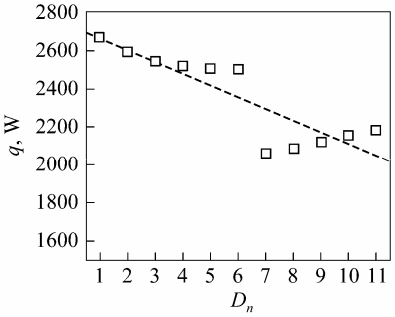


**Figure 4 Discrete heat flux and linear fit**
($\omega$=300rad·s$^{-1}$, $R_\mathrm{i}$=20mm, $R_\mathrm{o}$=30mm, $R_\mathrm{g}$=25mm, $B$=0.5, $h_\mathrm{i}$=1.5μm, $h_\mathrm{g}$=5μm, $\beta$=0.002rad)
□ heat flux; - - - - linear fit

Introducing $\overline{y}$ for the average value of $y_i$ and $\overline{q}$ for the average value of $q_i$, the linear regression equation $q(y)$:

$$q(y) = \hat{a}y + \hat{b} \tag{10}$$

which can be obtained by means of the least square method, with

$$\hat{a} = \frac{S_{yq}}{S_{yy}},\quad \hat{b} = \overline{q} - \hat{a}\overline{y},\quad S_{yy} = \sum_{i=1}^{n}(y_i - \overline{y})^2,$$

$$S_{qq} = \sum_{i=1}^{n}(q_i - \overline{q})^2,\quad S_{yq} = \sum_{i=1}^{n}(y_i - \overline{y})(q_i - \overline{q})$$

Hence, $B_i$ was solved and the temperature distribution became

$$T(x,y) = \frac{2\delta}{\lambda}\sum_{i=1}^{\infty}\Delta\left(\mathrm{e}^{k_i x} + \mathrm{e}^{-k_i x}\right)\cos k_i y + T_0 \tag{11}$$

where

$$\Delta = \frac{\hat{a}\cos nk_i - \hat{a} + k_i\left(\hat{a}n + \hat{b}\right)\sin nk_i}{k_i^2\left(\mathrm{e}^{k_i m} - \mathrm{e}^{-k_i m}\right)\left(k_i n + \sin k_i n\cos k_i n\right)}$$

## 2.4 Heat distribution ratio

The heat transfer coefficients from the outer surfaces of rotating ring and stationary ring to sealed medium $\alpha_1$ and $\alpha_2$ can be calculated by Eqs.(12) and (13)[12], respectively.

$$\alpha_1 = 0.135\lambda\left[\left(0.5Re_\mathrm{c}^2 + Re_\mathrm{a}^2\right)Pr\right]^{0.33}\Big/D_\mathrm{r} \tag{12}$$

$$\alpha_2 = 0.0115\lambda\varepsilon_1 Re^{0.8}Pr^{0.4}\Big/S_\mathrm{s} \tag{13}$$

where $Re_\mathrm{c} = \omega D_\mathrm{r}^2/\nu$, $Re_\mathrm{a} = UD_\mathrm{r}/\nu$ and $Re = 2VS_\mathrm{s}/\nu$. $U$ and $V$ are the sealed medium velocity along axis $x$ around rotating ring and stationary ring respectively.

The heat quantity $Q_1$ and $Q_2$ transferred by the two rings can approximately be calculated by Eqs.(14) and (15):

$$Q_1 = A_1\alpha_\mathrm{f}(T_\mathrm{f} - T_1) \tag{14}$$

$$Q_2 = A_2\alpha_\mathrm{f}(T_\mathrm{f} - T_2) \tag{15}$$

The heat transfer coefficient from fluid film to end faces $\alpha_\mathrm{f}$ can be calculated by Eq.(16)[18]:

$$\alpha_\mathrm{f} = 0.664\lambda_\mathrm{m}Pr^{0.33}\left(\frac{u_\mathrm{f}}{\nu L_\mathrm{c}}\right)^{0.5} \tag{16}$$

where $L_\mathrm{c} = \pi(R_\mathrm{o} + R_\mathrm{i})$ and $u_\mathrm{f} = (R_\mathrm{o} + R_\mathrm{i})\omega/4$.

The relationship between the heat quantity conducted by each ring and the average temperature on its end face can be expressed by Eqs.(17) and (18) according to Ref.[12]:

$$Q_1 = \zeta_1\lambda_1 A_1\tanh(\zeta_1 m_1)T_1 \tag{17}$$

$$Q_2 = \zeta_2\lambda_2 A_2\tanh(\zeta_2 m_2)T_2 \tag{18}$$

where $\zeta_1 = \sqrt{\alpha_1 L_1/(A_1\lambda_1)}$ and $\zeta_2 = \sqrt{\alpha_2 L_2/(A_2\lambda_2)}$.

Hence the heat distribution ratios $\delta_1$ and $\delta_2$ can be calculated by Eqs.(19) and (20), respectively, which were obtained from Eqs.(14), (15), (17) and (18).

$$\delta_1 = \frac{A_1 z_1(z_2 + \alpha_\mathrm{f}A_2)}{(A_1 + A_2)z_1 z_2 + (z_1 + z_2)A_1 A_2\alpha_\mathrm{f}} \tag{19}$$

$$\delta_2 = \frac{A_2 z_2(z_1 + \alpha_\mathrm{f}A_1)}{(A_1 + A_2)z_1 z_2 + (z_1 + z_2)A_1 A_2\alpha_\mathrm{f}} \tag{20}$$

where $z_1=\zeta_1\lambda_1 A_1\tanh(\zeta_1 L_1)$ and $z_2=\zeta_2\lambda_2 A_2\tanh(\zeta_2 L_2)$.

## 2.5 Temperature distribution of fluid film

Based on the assumption that the frictional heat was conducted by the two rings, the energy governing Eq. (21) for the fluid film reads[15]

$$\lambda_\mathrm{m}\frac{\partial^2 T}{\partial x^2} + \mu_{(T_\mathrm{m})}\left(\frac{\partial u}{\partial x}\right)^2 = 0 \tag{21}$$

where $\partial u/\partial x$ is the velocity gradient of fluid along axis $x$. $T$ can be obtained by integrating Eq.(21) twice and applying the temperature boundary conditions on the end faces which can be acquired from Eq.(11). Hence the temperature distribution equation is

$$T(x,y)=-\frac{\mu_{(T_m)}\omega^2(R_i+y)^2}{2\lambda_m(h_i+y\tan\beta)^2}x^2+\left[\frac{T_2(y)-T_1(y)}{h_i+y\tan\beta}+\frac{\mu_{(T_m)}\omega^2(R_i+y)^2}{2\lambda_m(h_i+y\tan\beta)}\right]x+T_1(y) \tag{22}$$

The local mean temperature is

$$T_m(y)=\sum_{i=1}^{\infty}f(\delta_1,\lambda_1,k_{1,i},m_1,n_1)\cos k_{1,i}y+\sum_{i=1}^{\infty}f(\delta_2,\lambda_2,k_{2,i},m_2,n_2)\cos k_{2,i}y+\frac{\mu_{(T_m)}\omega^2(R_i+y)^2}{12\lambda_m}+T_0 \tag{23}$$

where

$$f(\delta,\lambda,k_i,m,n)=\frac{\delta}{\lambda}\frac{\hat{a}\cos nk_i-\hat{a}+k_i(\hat{a}n+\hat{b})\sin nk_i}{k_i^2(e^{k_im}-e^{-k_im})(k_in+\sin k_in\cos k_in)}(e^{k_im}+e^{-k_im})$$

## 3 DEFORMATION OF END FACE

When the medium pressure is relatively low, the deformation induced by pressure is much less than that by frictional heat. Hence the effect of medium pressure on the deformation is neglected. When the outside of the sealing rings are surrounded by medium, the axial heat expansion at inner radius is larger than that at outer radius. The end face deformation can be expressed by the relative axial displacement $\Delta x$ between the outer and inner radius. Considering $\Delta x \ll n$, the following approximation:

$$\beta\approx\frac{\Delta x_1}{n}+\frac{\Delta x_2}{n} \tag{24}$$

holds, where $\Delta x_1$ and $\Delta x_2$ are the relative axial displacements of rotating ring and stationary ring respectively.

By using the finite element software ABAQUS, the model of the sealing rings can be built. The linear thermal flux of the fluid film was loaded on the end face by a subroutine which is called by ABAQUS CAE. The load of other boundary conditions and the definition of material can be easily realized in ABAQUS. $\Delta x$ can be read from the output file. For the sealing rings made of stainless steel 316L and carbine graphite, some calculation samples of $\Delta x$ are listed in Table 2.

**Table 2 Thermal deformation of sealing rings**

| $\omega$, rad·s$^{-1}$ | $h_i$, μm | $\Delta x$, μm | |
|---|---|---|---|
| | | 316L | Carbine graphite |
| 300 | 1.0 | 2.5 | 1.5 |
| 500 | 1.0 | 5.9 | 2.9 |
| 500 | 3.0 | 3.3 | 1.7 |

Note: $R_i$=20mm, $R_o$=30mm, $R_g$=25mm, $B$=0.5, $h_g$=5μm.

This method is accurate but time-consuming. By means of back propagation artificial neural nets (BP ANN), an efficient method was found to predict the deformation. A three-layer BP ANN was built which was composed of input layer for heat flux on all nodes on the end face in the radial direction, mid layer of 10 nodes and output layer for $\Delta x$. The relationship between the heat flux $q(y)$ and $\Delta x$ was established.

The input samples are the heat flux exerted on the nodes of end face. The heat flux is related to three factors, such as the viscosity, the fluid film thickness and the rotational speed, which can be selected according to orthogonal design[19,20]. The table of orthogonal design for the selection of the three factors is $L_{25}(5^6)$. Each factor has five levels, as Table 3 lists.

**Table 3 Factors and values of orthogonal design**

| Level | $\omega$, rad·s$^{-1}$ | $h_i$, μm | $\beta$, rad |
|---|---|---|---|
| 1 | 100 | 1.0 | 0.0001 |
| 2 | 300 | 1.5 | 0.0002 |
| 3 | 500 | 2.0 | 0.0003 |
| 4 | 700 | 2.5 | 0.0004 |
| 5 | 900 | 3.0 | 0.0005 |

It was found that the BP ANN can calculate the deformation satisfactorily by comparing some results of $\Delta x$ calculated by BP ANN with that did by ABAQUS. The fore treatment and after treatment of ABAQUS CAE cost much more time than BP ANN, and the BP ANN is an more efficient and convenient method.

## 4 CHARACTERISTICS OF FLUID FILM

The fluid flow between the end faces was regarded as laminar flow of viscous liquid, which can be described by Reynolds equation in cylindrical coordinates for incompressible fluid[17]:

$$\frac{\partial}{r\partial r}\left(\frac{h^3r}{\mu}\frac{\partial p}{\partial r}\right)+\frac{\partial}{r\partial\theta}\left(\frac{h^3}{\mu}\frac{\partial p}{r\partial\theta}\right)=6\omega r\frac{\partial h}{r\partial\theta} \tag{25}$$

where $h$ is the fluid film thickness, $r$ and $\theta$ are the radial and circumferential coordinates, respectively. By using Galerkin weighted residual method with second-order shape functions, a finite element program was developed to solve Eq.(25) numerically. A periodic weir and groove area was part of the solution domain as Fig.5 illustrates, where $\varphi$ is a transferred coordinate, $\varphi=\ln R_i+\theta\tan\alpha$, $N$ is the total number of nodes.

The pressure and velocity distributions of the fluid film were calculated by the finite element program. Therefore, the main sealing performance parameters were obtained, including the bearing force of the fluid film, the leakage rate and the frictional torque. For instance, Fig.6 illustrates the pressure nephogram of a periodic domain of fluid film when $\omega$=300rad·s$^{-1}$, $R_i$=20mm, $R_o$=30mm, $R_g$=25mm, $B$=0.5, $h_i$=1.5μm, $h_g$=5μm and $\beta$=0, where $P=(p-p_i)/(p_o-p_i)$. There exists a high-pressure area near the end radius of spiral groove and accordingly, the bearing force is increased, that's the results of hydrodynamic effect.

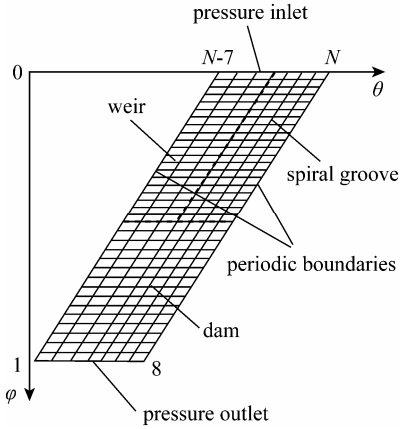


**Figure 5 Mesh of solution domain**

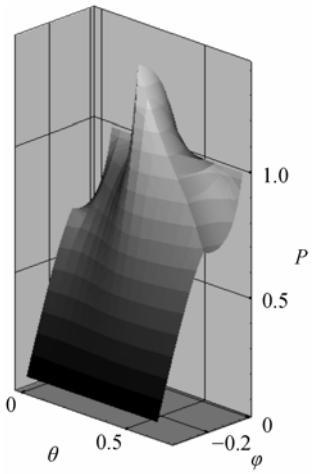


**Figure 6 Pressure distribution in fluid film**

## 5 OPTIMUM DESIGN

### 5.1 Determination of primary parameters of sealing rings

The primary parameters of sealing rings were determined according to the design objective of reducing the temperature of sealing rings.

The radial width of end face $n$ heavily influences the quantity of frictional heat. When $R_i$ is constant, the larger the width, the larger the frictional heat quantity is, and the larger the heat-transfer area of the outer surface of sealing ring is. The calculated temperature field of the sealing members and the fluid film indicates that the highest temperature $T_{max}$ locates at the inner radius of fluid film next to the rotating ring. The heat flux $q=2000\text{W}\cdot\text{m}^{-1}$ was specified on the end face to investigate the change of $T_{max}$ with $m$ and $n$, $R_i=20$mm. As illustrated in Fig.7, when $n$ is less than 8mm, the increase of cooling area results in the reduction of $T_{max}$; but once $n$ is larger than 8mm, the radial temperature gradient increases and $T_{max}$ rises accordingly. Therefore, there exists an optimal width of the seal face corresponding to the minimal $T_{max}$.

The length $m$ has less evident influence on $T_{max}$ than $n$. $T_{max}$ always decreases with the increase of $m$ because the increase of $m$ enlarges the heat-transfer area but does not change the frictional heat, as shown in Fig.7 for the case with $n=5$mm. The effect of $m$ on $T_{max}$ is nearly negligible when $m>11$mm.

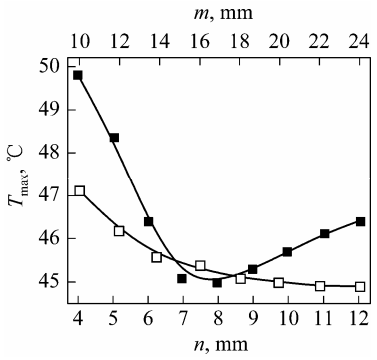


**Figure 7 Variation of $T_{max}$ with $m$ and $n$**
■ $n$; □ $m$

Another important parameter is the coefficient of heat conductivity of the rotating ring $\lambda$. The coefficient $\lambda$ of the frequently used materials for mechanical seals ranges from 15 to $100\text{W}\cdot\text{m}^{-1}\cdot\text{K}^{-1}$. When $\lambda=15\text{W}\cdot\text{m}^{-1}\cdot\text{K}^{-1}$, $T_{max}$ is about 46℃, and when $\lambda=100\text{W}\cdot\text{m}^{-1}\cdot\text{K}^{-1}$, $T_{max}=26$℃ under the conditions that $\omega=500\text{rad}\cdot\text{s}^{-1}$, $h_i=1.0\mu$m, $m=8$mm and $n=11$mm. It can be seen that the large coefficient $\lambda$ can effectively lower the temperature of sealing rings.

The coefficients $\alpha_1$ and $\alpha_2$ were calculated according to Eqs.(12) and (13), as illustrated in Fig.8. The coefficient $\alpha_1$ increases obviously with the increase of $\omega$. For the medium is circled and its temperature $T_0$ remains constant, the axial velocity of the medium around the stationary ring increases slightly with $\omega$ and results in the small variation of $\alpha_2$. The heat distribution ratios $\delta_1$ and $\delta_2$ are mainly related to $\alpha_1$ and $\alpha_2$. Because $\alpha_1$ is much larger than $\alpha_2$, most of the frictional heat is conducted by the rotating ring.

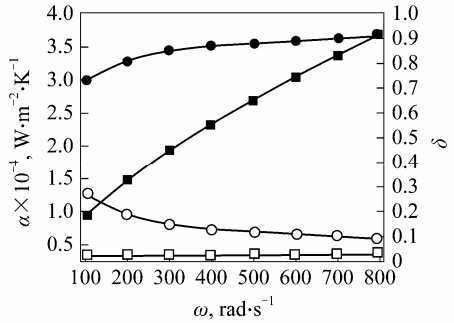


**Figure 8 Values of $\alpha$ and $\delta$ corresponding to $\omega$**
($D_r=30$mm, $U=V=0.5\text{m}\cdot\text{s}^{-1}$, $S_s=0.15$m)
■ $\alpha_1$; □ $\alpha_2$; ● $\delta_1$; ○ $\delta_2$

### 5.2 Optimum design of spiral groove parameters

The fluid film provides the bearing force to open the two end faces, meanwhile the leakage rate should be less than the allowable value. Therefore, the large bearing force was regarded as the design objective and the permissible leakage rate regarded as a constraint condition. Under the given operation conditions, the variables which affect the design objective include $\alpha$, $N_g$, $h_g$, $B$ and $\bar{R}_g$, as Eq.(26) expressed.

$$f = f\left(\alpha, N_g, h_g, B, \bar{R}_g\right) \tag{26}$$

where

$$\begin{cases} 0 \leqslant \alpha \leqslant 1.736 \text{ rad} \\ 8 \leqslant N_g \leqslant 20, \quad N_g \text{ should be integer} \\ 0.5 \leqslant h_g \leqslant 20 \text{ μm} \\ 0.1 \leqslant B \leqslant 0.9 \\ 0.1 \leqslant \bar{R}_g \leqslant 0.9 \end{cases} \tag{27}$$

The optimum design of spiral groove is a nonlinear, constrained optimization problem, which was solved by the complex method. Its process consists of two modules. One is to improve the geometrical parameters of spiral groove by the complex method. The other is to evaluate the value of the objective function by using the method depicted in Section 4. The optimized parameters of spiral groove are listed in Table 4. In this example, the fluid film thickness in non-groove area $h_1$ was assumed to be 3μm, $R_i$=20mm, $R_o$=30mm.

**Table 4 Parameters of the spiral grooves**

| $\alpha$, rad | $N_g$ | $h_g$, μm | $B$ | $\bar{R}_g$ |
|---|---|---|---|---|
| 0.14 | 12 | 6.2 | 0.7 | 0.6 |

The parameter $h_1$ should be controlled in consideration of two requirements, namely both good fluid lubrication of the two end faces and small leakage rate. The relationship between $h_g$ and $h_1$ was expressed by the parameter $H$:

$$H = 1 + \frac{h_g}{h_1} = 3 \tag{28}$$

The parameter $H$ heavily influences the hydrodynamic effect of spiral grooves[17]. By using the parameters in Table 4, when $\omega$=500rad·s$^{-1}$, the bearing force is 2873 N and the leakage rate is $2.2\times10^{-8}$m$^3$·s$^{-1}$.

### 5.3 Coupling analysis of frictional heat and thermal deformation

In order to determine the value of $\beta$ corresponding to $\omega$ and $h_i$, the coupling analysis was carried out in consideration of the viscosity change with the fluid film temperature. A coupling analysis program was developed to search for $\beta$ by iterative computation. Because the frictional heat decreases with the increase of $\beta$ according to Eq.(4), and $\beta$ increases with the increase of the frictional heat according to thermal deformation calculation, there exists the unique optimal value of $\beta$ which meets the coupling requirements between the thermal deformation and the frictional heat flux. In each iteration step, the temperature and viscosity of fluid film were calculated according to Eqs.(23) and (5). The viscosity increases with the increase of $\beta$, namely if $\beta$ is enlarged, the viscosity increases too, and the frictional heat is enlarged. The values of $\beta$ corresponding to different $h_i$ and $\omega$ were obtained and illustrated in Fig.9.

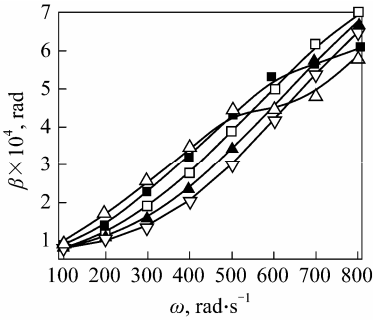


**Figure 9 Values of $\beta$ corresponding to given $h_i$ and $\omega$**
$h_i$, μm: △ 0.5; ■ 1.0; □ 2.0; ▲ 3.0; ▽ 4.0

### 5.4 Reshaping of spiral groove

When $h_i$=3μm and $\omega$=500rad·s$^{-1}$, $\beta$ is equal to $3.5\times10^{-4}$ rad. The bearing force is 2312 N, and the volume leakage rate is equal to $2.4\times10^{-8}$m$^3$·s$^{-1}$. It is obvious that the deformation decreases the bearing force but increases the leakage rate.

Once $h_1$ varies along radius, $H$ is not constant and the bearing force of fluid film decreases. It was found that the hydrodynamic effect will not change if $H$ does not various along radius. That means the bearing force of the fluid film will not change. To obtain the results, $h_g$ should be the function of $r$, as Eq.(29) expresses.

$$h_g = \frac{H}{1-H}\left[h_i + \left(r - R_i\right)\tan\beta\right] \tag{29}$$

The groove depth increases continuously from the end of groove to outer radius, and with this reshaping of spiral groove, the bearing force increases to 2660 N.

### 5.5 Reshaping of sealing dam

If the size of the gap between the two end faces does not change along radius, namely the gap is a radial parallel gap, the fluid film is relatively stable and the leakage rate is small[17]. To obtain a parallel gap, the two end faces were prefabricated to form a divergent gap in dam area, as illustrated in Fig.10(a). The divergent angle $\beta_1$ should equal to the convergent angle $\beta_2$ composed of the two deformed end faces, namely the thermal deformation of the end faces is offset by the prefabrication. The two deformed end faces form a parallel gap when the thermal deformation takes place, as illustrated in Fig.10(b).

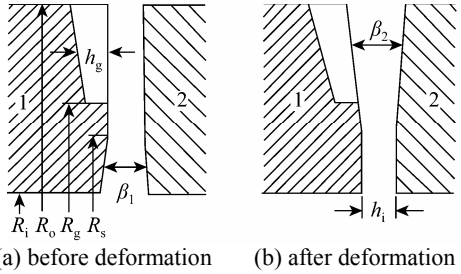


(a) before deformation (b) after deformation

**Figure 10 Gap models in end faces**
1—rotating ring; 2—stationary ring

The leakage rate is related to the reshaping location $R_s$. $R_s$ should be smaller than $R_g$ because the end faces of mechanical seal should contact closely to seal medium when the mechanical seal rests. $R_s$ was suggested to be 22mm in this example, and $\beta_1$ was $8\times10^{-4}$ rad.

After the reshaping, the bearing force of fluid film equaled to 2612 N, and the volume leakage rate equaled to $1.6\times10^{-8}$m$^3\cdot$s$^{-1}$. It is indicated that the bearing force of fluid film is increased and the leakage rate is reduced by reshaping the sealing members. The sealing performance parameters of the spiral groove mechanical seal before and after optimum design are listed in Table 5. By the new method put forward in this paper, the aggregative evaluating indicator $F/Q$ can be improved significantly.

**Table 5 Parameters of sealing performance**

| | $F$, N | $Q\times10^8$, m$^3\cdot$s$^{-1}$ | $F/Q$, N$\cdot$m$^{-3}\cdot$s |
|---|---|---|---|
| ideal parallel gap | 2873 | 2.2 | $1305\times10^8$ |
| deformed convergent gap | 2312 | 2.4 | $963\times10^8$ |
| reshaped convergent gap | 2612 | 1.6 | $1633\times10^8$ |

## 6 CONCLUSIONS

Since it heavily changes the characteristics of fluid film, such as the bearing force and the leakage rate, the frictional heat of fluid film was considered in the deign of spiral groove mechanical seal. When the fluid film thickness at inner radius and the rotational speed are given, there exists the compatible relationship among the separation angle of the two deformed end faces, the frictional heat, the viscosity and the temperature of fluid film. The bearing force decreases but the leakage rate increases when the thermal deformation takes place.

The appropriate primary dimensions of sealing rings, such as the radial width and the axial length, were determined according to heat transfer analysis, which result in the minimal temperature on end faces. The parameters of spiral groove were optimized by regarding the large bearing force as the design objective. To minimize the effect of thermal deformation on the sealing performance, the spiral grooves and the sealing dam were reshaped. The groove depth increased from the end radius of groove and the sealing dam was prefabricated to form a divergent gap. Hence the hydrodynamic effect of spiral grooves was improved and the leakage rate was reduced by the parallel gap in the sealing dam under operation condition.

## NOMENCLATURE

$A$ area of end face, mm$^2$
$B$ ratio of circumferential width of spiral groove to that of a periodic weir and groove
$C$ specific heat, J$\cdot$kg$^{-1}\cdot$K$^{-1}$
$D_r$ diameter of rotating ring, mm
$E$ Young's modulus, GPa
$h$ thickness of fluid film, μm
$h_g$ depth of spiral groove, μm
$h_i$ thickness of fluid film at inner radius, μm
$L$ circumference of seal ring, mm
$m$ length of seal ring, mm
$N_g$ number of spiral grooves
$n$ width of seal ring, mm
$Pr$ Prandtl number
$p$ pressure of fluid film, MPa
$p_o$ operating pressure, MPa
$q$ frictional heat flux, W$\cdot$m$^{-2}$
$R_g$ end radius of spiral groove, mm
$\bar{R}_g$ dimensionless parameter, $\bar{R}_g=(R_g-R_i)/(R_o-R_i)$
$R_i$ inner radius of fluid film, mm
$R_o$ outer radius of fluid film, mm
$r$ radius of fluid film, mm
$S_s$ distance from outer surface of stationary ring to the inner surface of sealing chamber, mm
$T$ temperature, ℃
$T_m$ average temperature of fluid film, ℃
$T_0$ temperature of sealed medium, ℃
$T_1$ average temperature of end face of rotating ring, ℃
$T_2$ average temperature of end face of stationary ring, ℃
$U$ axial flow velocity of sealed medium around rotating ring, m$\cdot$s$^{-1}$
$u$ tangential velocity of fluid film, m$\cdot$s$^{-1}$
$V$ axial flow velocity of sealed medium around stationary ring, m$\cdot$s$^{-1}$
$\alpha$ spiral angle, rad
$\alpha_f$ heat transfer coefficient from fluid film to end face of sealing rings, W$\cdot$m$^{-2}\cdot$K$^{-1}$
$\alpha_i$ heat transfer coefficient from sealing ring to sealed medium, W$\cdot$m$^{-2}\cdot$K$^{-1}$
$\alpha_1$ heat transfer coefficient from rotating ring to sealed medium, W$\cdot$m$^{-2}\cdot$K$^{-1}$
$\alpha_2$ heat transfer coefficient from stationary ring to sealed medium, W$\cdot$m$^{-2}\cdot$K$^{-1}$
$\beta$ separation angle of two deformed end faces, rad
$\delta$ heat distribution ratio
$\varepsilon$ Poisson's ratio
$\varepsilon_1$ correction factor ($\varepsilon_1=2$)
$\lambda$ coefficient of heat conductivity of sealing ring, W$\cdot$m$^{-1}\cdot$K$^{-1}$
$\lambda_m$ coefficient of heat conductivity of sealed medium, W$\cdot$m$^{-1}\cdot$K$^{-1}$
$\mu$ dynamic viscosity, kg$\cdot$m$^{-1}\cdot$s$^{-1}$
$\nu$ kinematic viscosity, m$^2\cdot$s$^{-1}$
$\tau$ coefficient of thermal expansion
$\omega$ rotation speed, rad$\cdot$s$^{-1}$

## REFERENCES

1 Etsion, I., "A New conception of zero-leakage non-contacting face seal", *J. Trib.*, **106**(3), 338—343 (1984).
2 Lai, T., "Development of non-contacting, non-leakage spiral groove liquid face seals", *Lubrication Eng.*, **50**(8), 625—631(1994).
3 Zeus, D., "Viscous friction in small gaps calculations for non-contacting liquid or gas lubricated end face seals", *Trib. Trans.*, **33**(3), 454—462(1990).
4 Sato, Y., Ono, K., Iwama, A., "Optimum groove geometry for spiral groove viscous pumps", *J. Trib.*, **112**, 409—414(1990).
5 Sato, Y., Knight, J.D., "Performance characteristics of shrouded rayleigh-step and spiral groove viscous pumps", *J. Trib.*, **114**, 499—507(1992).
6 Zhao, Y., Song, P.Y., Li, W., Cao, D.F., "Operation characteristics of spiral groove gas face seal at the slow

speed-theory analysis", *Lubrication Eng*., **9**, 70—73(2005). (in Chinese)
7 Faria, M.T.C., "An efficient finite element procedure for analysis of high-speed spiral groove gas Face seals", *J. Trib*., **123**(1), 205—210(2001).
8 Furuishi, Y., Suganami, T., Yamamoto, S., Tokumitsu, K., "Performance of water-lubricated flat spiral groove bearings", *J. Trib*., **107**, 268—273(1985).
9 Larsson, B., "Heat separation in frictional rotor-seal contact", *J. Trib*., **102**(3), 600—607(2003).
10 Cicone, T., Pascovici, M.D., Tournerie, B., "Non-isothermal performance characteristics of fluid film mechanical face seals", *J. Eng. Trib*., **215**(1), 35—44(2001).
11 Zhou, J.F., Gu, B.Q., "Heat-transfer character analysis of rings of mechanical seal", *Chinese J. Mech. Eng*., **42**(9), 201—206(2006). (in Chinese)
12 Peng, X.D., Xie, Y.B., Gu, Y.Q., "Determination of the end face temperature of mechanical seal", *Chem. Mach*., **23**(6), 333—336(1996). (in Chinese)
13 Pascovici, M.D., "Temperature distribution in the lubrication film of sliding bearings under intensive lubrication-wall heat transfer condition", *Wear*, **29**, 277—286(1974).
14 Brunetiere, N., Tournerie, B., Frene, J., "A simple and easy-to-use TEHD model for non-contacting liquid face seals", *Trib. Trans*., **46**(2), 187—192(2003).
15 Pascovici, M.D., Etison, I., "Thermo-hydrodynamic analysis of a mechanical face seal", *J. Trib*., **114**(4), 639—645(1992).
16 Dumbrava, M.A., Morariu, Z., "Thermohydrodynamic aspects of the double mechanical seals", In: Proc. 11th international conference on fluid sealing, British Hydromechanics Research Association (BHRA), 394—406(1987).
17 Zhou, J.F., "Study on thermo-hydrodynamic effect in mechanical seals", Ph.D. Thesis, Nanjing Univ. of Tech., China (2006). (in Chinese)
18 Ren, Y., Zhang, H., Heat Transfer Theory, China Univ. of Petroleum Press, Beijing, 48—49(1988). (in Chinese)
19 Tasy, S., Hong, P., Chieu, B., "Handwritten digit recognition *via* neural network by selective pruning", In: IEEE Proc, 11th Int. Conf. Pattern Recognition, 656—659(1992).
20 Choueiki, M.H., Mount-Campbell, C.A., "Training data development with the D-optimality criterion", *IEEE Trans. Neural Networks*, **10**, 56—63(1999).